23rd ABCM International Congress of Mechanical Engineering
December 6-11, 2015, Rio de Janeiro, RJ, Brazil

ANALYSIS OF THE GEOMETRIC NONLINEAR EFFECT ON THE MECHANICAL BEHAVIOR OF PSEUDOELASTIC SHAPE MEMORY ALLOY HELICAL SPRINGS

Marcelo Amorim Savi
Mauricio S. Garcia
Universidade Federal do Rio de Janeiro - COPPE – Department of Mechanical Engineering
P.O. Box 68.503 - 21.941.972 – Rio de Janeiro – RJ – Brazil
savi@mecanica.ufrj.br, mauriciogarc@gmail.com

Pedro Manuel Calas Lopes Pacheco
Ricardo Alexandre Amar de Aguiar
Luís Felipe Guimarães de Souza
Rodolpho Barbosa da Hora
CEFET/RJ – Centro Federal de Educação Tecnológica Celso Suckow da Fonseca - Department of Mechanical Engineering
20.271.110 - Rio de Janeiro - RJ – Brazil
calas@cefet-rj.br, raaguiar@cefet-rj.br, lfelipe@cefet-rj.br, rodolphodahora@gmail.com

Abstract. *Due to the special characteristics of Shape Memory Alloys (SMAs), several industrial applications are developed in areas such as aeronautics, medicine and robotics. SMA actuators are being employed as an alternative to electric, hydraulic and pneumatic actuators, and also, in response to a growing need to develop smaller and lighter systems. In this regard, the use of SMAs is increasing in different fields of human knowledge due to its good power-weight ratio. This paper deals with an investigation of nonlinear geometric effect on the mechanical behavior of pseudoelastic shape memory alloy (SMA) helical springs. Initially, SMA wires characterization is presented. Afterward, a discussion about the design and fabrication of SMA helical springs are performed. Experimental tensile tests are then carried out showing the nonlinear geometric influence. Results show a coupling between constitutive and geometric nonlinearities that defines the spring stiffness. Two springs with different geometries are built from SMA wires, defining springs with weak and strong nonlinear geometric influence. Numerical analysis is developed employing the finite element method confirming the general conclusions showed in experimental observations.*

Keywords: *shape memory alloys, pseudoelasticity, spring, geometric nonlinearities, finite element analysis*

1. INTRODUCTION

Shape Memory Alloys (SMAs) present complex thermomechanical behaviors related to different physical processes. The most common phenomena presented by this class of material are the pseudoelasticity, the shape memory effect, which may be one-way (SME) or two-way (TWSME), and the phase transformation due to temperature variation. SMA unique properties are due to solid phase transformations that can be induced either by stresses or by temperature. The remarkable properties of SMAs are attracting much technological interest, motivating different applications in several fields of sciences and engineering (Machado and Savi, 2003; Bundhoo *et al.*, 2009; Hartl *et al.*, 2010; Spinella and Dragoni, 2010; Min An *et al.*, 2012). SMA elements can be designed using wires, beams, and plates, among other possibilities. Several industrial applications were established in areas such as aeronautics, medicine and robotics.

SMA springs constitute an alternative for applications where large displacements are needed, being of special relevance concerning dynamical applications. A mechanical helical spring may be defined as a body with the ability to bend, warp or absorb energy when subjected to a load (Shigley, 2011).

The macroscopic mechanical behavior of SMA springs is better expressed by force-displacement (F-u) curves that have similar characteristics of stress-strain (σ-ε) curves associated with tensile tests of wires and bars. Figure 1 presents schematic pictures of both curves showing the classical pseudoelastic behavior. It is noticeable a linear elastic region, associated with austenitic phase, followed by a phase transformation plateau. Afterward, there is a new linear elastic region associated with martensitic phase. The slope of each linear region of the stress-strain curve defines the elastic modulus. Analogously, the slope of the linear region of the force-displacement curve defines the spring stiffness. Hence, two different parameters are usually defined: E_A and E_M, respectively the austenitic and martensitic elastic modulus of wires or bars; K_A and K_M, respectively the austenitic and martensitic spring element stiffness. In general, this general behavior is the same for other stress components and can be observed in torsion tests, defining shear elastic modulus. Usually, SMA has austenitic elastic modulus that can be four times larger than martensitic modulus.

Nevertheless, the stiffness of SMA helical springs is affected by the coupling of constitutive and geometrical nonlinearities effects, introducing changes in this usual mechanical description. The main goal of this paper is to establish a proper comprehension of the geometrical nonlinear effect on helical springs, mainly expressed by the spring stiffness.

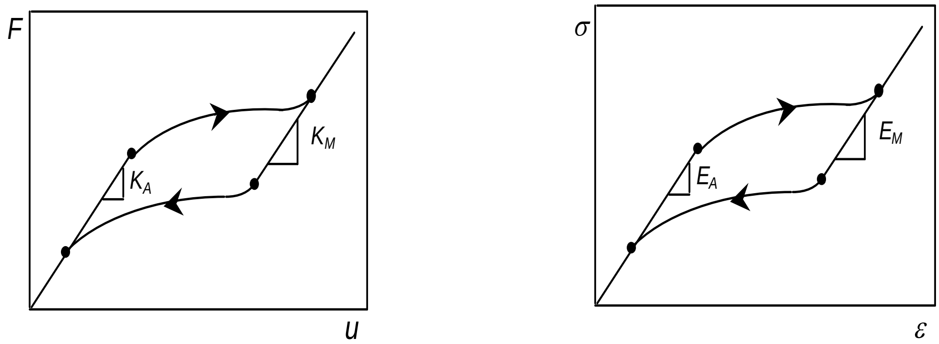

(a) (b)

Figure 1. SMA macroscopic pseudoelastic behavior represented by force-displacement curve for springs (a) and stress-strain curve for wires or bars (b).

SMA springs are being addressed in different forms in the literature. Attanasi *et al.* (2011) investigated the behavior of pseudoelastic SMA springs to verify the feasibility of their use in devices where the restitution force exceeds the linear limit. Experimental tests were conducted considering prescribed displacements. Case *et al.* (2004) described procedures for training SMAs, considering thermally induced process that occurs when the alloy is heated to temperatures of approximately 500°C by interval time from 10 to 25 minutes.

Mathematical modeling of the thermomechanical behavior of SMAs helical springs is also the objective of several researches. Tobushi and Tanaka (1991) proposed a simplified model where each small segment of the pure spring is subjected to torsion. Liang and Rogers (1997) proposed a nonlinear thermomechanical model for springs employed in vibration control. Toi *et al.* (2004) presented a model using finite element formulation of the Timoshenko beam and the Brinson's model for SMA description. Aguiar *et al.* (2010) developed a model for SMA spring based on the model proposed by Paiva *et al.* (2005). Numerical simulations are in close agreement with experimental data for different temperatures. Sung-Min *et al.* (2012) developed a simplified model considering two states: austenite and martensite. Some geometric effects, such as reducing the diameter of the spring, are analyzed.

This work deals with an investigation of the nonlinear geometric influence on the mechanical behavior of SMA helical springs. Experimental and numerical approaches are employed. In this regard, two different springs built with distinct geometrical characteristics are designed in order to change phase transformation conditions. Both springs are produced from the same SMA wire. The main point is that one spring presents phase transformation related to small displacements while the other presents large displacements. A comparison between results of both springs subjected to tensile tests is presented, establishing a proper comprehension about geometric influence. Finite element analysis is employed to confirm the experimental observations.

2. EXPERIEMENTAL PROCEDURE

Helical springs are manufactured from austenitic NiTi wires of 1.7 mm (0.066 in). The manufacturing process consists of a mechanical conformation stage followed by a heat treatment process of the coiled wire to maintain the austenitic characteristics and the desired shape at the room temperature.

2.1. NiTi wire Characterization

Prior to the manufacturing process, differential scanning calorimeter tests (DSC) and tensile tests are developed to characterize the NiTi wire (Savi *et al.*, 2015). The following phase transformation temperatures are obtained from DSC tests: A_s = 16.7°C, A_f = 30.2°C, M_s = 24.8°C, M_f = 9.1°C. A_s and A_f are, respectively, start and finish of austenite transformation temperatures, whereas M_s and M_f, are the start and finish of martensite transformation temperatures. Pseudoelastic tensile tests at room temperature are used to obtain the wire elastic modulus associated to austenitic and martensitic volumetric phases. The following values are estimated: E_A = 46 GPa, E_M = 22 GPa. Based on that, it is possible to observe a difference around 50% between both elastic moduli. The shear modulus is defined as $G = \frac{E}{2(1+\upsilon)}$ where ν is the Poisson ratio. Note that there is a direct relation between elastic and shear moduli. By assuming a Poison ratio of 0.3, it is possible to estimate shear modulus: G_A = 17.7 GPa and G_M = 8.5 GPa.

2.2. Helical Springs Manufacturing

Spring is a mechanical element characterized by high flexibility being usually employed to store and to release energy. Helical springs resist and deflect under tensile or compressive loads (Shigley, 2011). Essentially, helical springs transforms axial force into torque and shear stress in the cross section of the spring. Three geometric parameters are usually considered for the design of a helical spring: wire diameter, d, average coil diameter, D, and number of active coils, N. Geometric nonlinear effects can dramatically change helical spring behavior when subjected to large displacements. This behavior affects an important design parameter known as spring index that establishes a relationship between coil and wire diameters, $C = D/d$.

In contrast of elastic helical springs, SMA helical springs present a nonlinear distribution of shear stress due to phase transformations. This behavior tends to produce even higher displacements when compared to elastic helical springs. This work has the objective to produce two SMA helical springs that present different nonlinear geometric characteristics: the first one has weak geometric nonlinearity, named W-Spring; while the second one has a strong geometric influence, named S-Spring. The linear approach is employed to define the spring characteristics (Sung-Min *et al.*, 2012). The idea is to produce, respectively, small and large displacements, for the same loading level. Table 1 summarizes characteristics of both springs.

Table 1. Spring parameters.

Parameters	W-Spring	S-Spring
Wire diameter (mm)	1.7	1.7
Coil diameter (mm)	10.5	13.8
Spring index (C)	6.2	8.1
Number of active coils	3	5

SMA helical spring manufacturing considers an SMA wire that is employed to build the spring with the aid of a device where shape is conformed, clamping the spring ends. Afterward, it is necessary to promote a heat treatment that defines the spring form as the natural one. This treatment is planned in order to promote the SMA recrystallization assuring a proper manufacturing of the spring. Here the conformed wires were heated at 500°C for 30 minutes and, in the sequence, a water cooling is performed (Savi *et al.*, 2015).

2.3. Helical Springs Tensile Tests

Tensile tests are performed to characterize the pseudoelastic behavior of SMA helical springs considering both W-Spring and S-Spring. Different test scenarios are conducted considering distinct maximum displacements for the same loading level. W-Spring: 5mm, 10mm, 25mm, 30mm, 35mm, and 40mm; S-Spring: 30mm, 45mm, 65mm, 80mm, 100mm and 120mm. A testing system INSTRON 5966 with 10 kN capacity equipped with a 1 kN loadcell is employed considering the prescribed displacement loading varying from zero to a maximum displacement value using a triangular shape wave with a loading rate of 100 mm/min. Figure 2 presents pictures of W-Spring and S-Spring test.

Stiffness is considered as the essential characteristics of the spring. It is defined from the slope of the linear elastic regions observed before (austenitic phase) and after (martensitic phase) the hysteresis plateau related to the stabilized experimental pseudoelastic curves. The stiffness associated with the austenitic phase is estimated during the loading stage considering the points in the region between 12% to 20% of the maximum load. On the other hand, the stiffness associated with the martensitic phase is obtained during the unloading stage considering the points in the region between 90% to 98% of the maximum load. This methodology reduces the influence of instability effects related to the load inversion stage.

(a) (b) (c) (d)

Figure 2. Maximum displacement configurations. W-Spring: (a) 25 mm; (b) 40 mm. S-Spring: (c) 65 mm; (d) 120 mm.

Figure 3 shows force-displacement curves obtained at room-temperature for the two springs considering different loadings. Pseudoelastic response of the springs is evident, showing the hysteretic behavior. Although the system has nonlinear characteristics, it is possible to use stiffness related to austenitic and martensitic phase to define mechanical aspects of the spring. Basically, it is considered the slope of the linear elastic regions, before and after the hysteresis plateau, being respectively related to austenitic and martensitic phases.

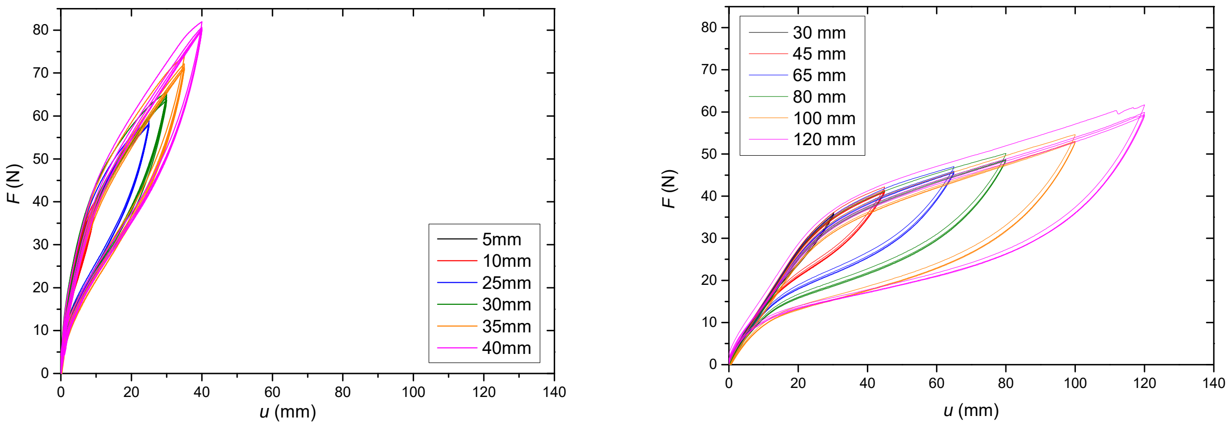

(a) (b)

Figure 3. Force-displacement curves: (a) W-Spring and (b) S-Spring.

Table 2 presents the summary of the stiffness average values for the different displacement levels. Note that for the W-Spring the slope of the elastic response at the austenitic phase is larger than the one in the martensitic phase. For the S-Spring the austenitic stiffness is smaller than the martensitic stiffness calculated from the slope of the martensitic region. Since the austenitic shear modulus is larger than the martensitic one, geometric nonlinearity can be pointed as responsible for the stiffness increase for the S-Spring.

Table 2 – Stiffness estimation of the W-Spring and S-Spring.

Stiffness average values	W-Spring	S-Spring
$\overline{K_A}$ (N/mm)	9.0	1.2
$\overline{K_M}$ (N/mm)	4.4	1.5
Δ (%)	- 50	+ 20

3. FINITE ELEMENT ANALYSIS

Numerical simulations are now in focus promoting a proper explanation about the experimental observations. A three-dimensional finite element model is employed to study the pseudoelastic behavior of SMA helical springs subjected to axial loadings. Geometrical nonlinearities are included in the analysis considering large displacement hypothesis. A commercial finite element code ANSYS (Ansys, 2012) is employed considering coupled thermal and mechanical fields element SOLID 186 for spatial discretization.

Constitutive nonlinearity is related to the SMA thermomechanical behavior and different constitutive models can be employed for this description. Lagoudas (2008) and Paiva & Savi (2006) presented an overview of constitutive models for SMAs. Here, the constitutive model proposed by Auricchio *et al.* (1997) is employed. This three-dimensional model is capable to describe the pseudoelastic behavior considering two phases: austenite (A) and martensite (M). The internal variables ξ_A and ξ_M are introduced to represent, respectively, austenitic and martensitic volume fractions that satisfies the following relation: $\xi_A + \xi_M = 1$. Hence, it is possible to use only one internal variable, $\xi = \xi_M = 1 - \xi_A$. The process of phase transformation is controlled by 4 critical stresses σ_s^{AM}, σ_f^{AM}, σ_s^{MA}, σ_f^{MA}, where s and f subscripts state for start and finish and AM represents austenite-martensite transformation whereas MA represents martensite-austenite transformation. It is important to highlight that this model uses the same elastic modulus for both austenite and martensite. Based on this restriction, all simulations are performed assuming the austenitic elastic modulus.

Although this model is not able to describe all complex details of SMA thermomechanical behavior, it is convenient for several purposes, allowing the description of important features employed for the design of SMA devices. Indeed, despite the limitations of the model employed in this work, comparisons with experimental data show that this SMA model properly captures the main behavior of pseudoelastic helical spring subjected to mechanical loadings.

The finite element analysis is carried out considering a solid model representing both the W-Spring and the S-Spring with a mesh obtained after a convergence analysis. Experimental situations are reproduced by considering proper boundary conditions involving displacement restrictions and loadings. Basically, it is assumed one end of the spring is fixed, prescribing null displacements for all degrees of freedom on its cross section area; the other end cross section is subjected to a prescribed load-unload cyclic displacement in the spring longitudinal direction. Variables distribution through the spring, as stress and volume fraction, are analyzed at a central section to avoid the effects of the loadings and prescribed boundary conditions at the two spring ends.

Numerical simulations are performed by considering parameters the following parameters: E = 46 GPa, ν = 0.30, σ_s^{AM}= 297 MPa, σ_f^{AM} = 772 MPa, σ_s^{MA} = 306 MPa, σ_f^{MA} = 78 MPa and ε_L = 0.07. In essence, these values are adjusted using the experimental data described in the preceding section.

Figure 4 shows a comparison between numerical and experimental data for W-Spring and S-Spring maximum loading displacements. Results show that model simulations capture the general behavior observed in experimental data. It should be highlighted that, since the constitutive SMA model considers the same elastic modulus for both austenitic and martensitic phases, numerical simulations have this restriction and do not capture the stiffness change. Nevertheless, results show that the proposed model is able to represent the behavior of the SMA helical spring.

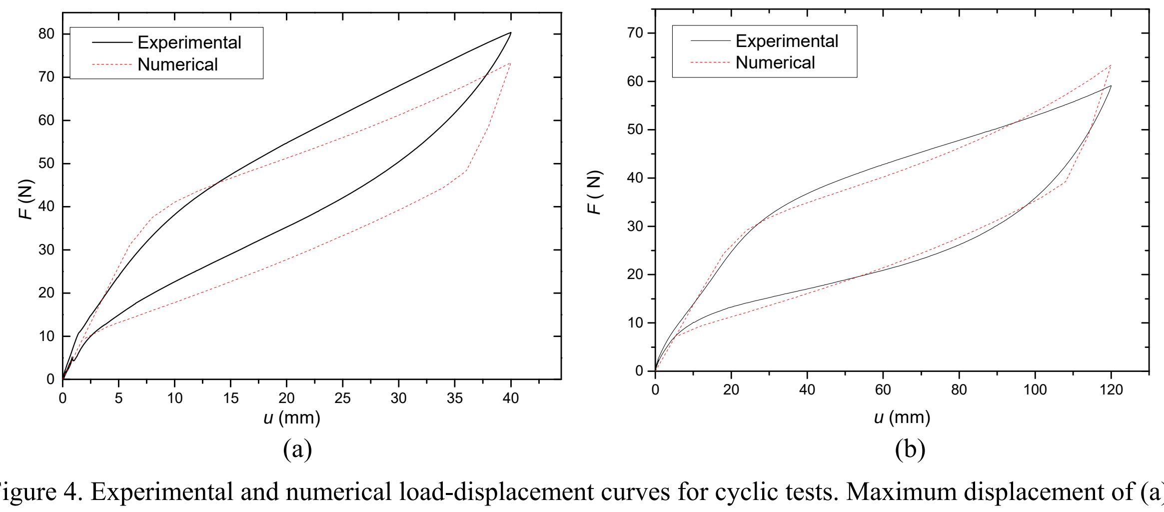

(a) (b)

Figure 4. Experimental and numerical load-displacement curves for cyclic tests. Maximum displacement of (a) 40 for W-Spring and (b) 120 mm for S-Spring.

Basically, the maximum displacements of the previous results are treated: W-Spring with 40 mm of maximum prescribed displacement and S-Spring with 120 mm of maximum prescribed displacement. In order to establish a proper comparison between both springs, it is chosen two situations that experiments similar values of *von Mises* equivalent stresses (600 MPa) and volume fractions (62%). Figure 5 shows SMA helical springs in initial and deformed configurations for both springs. As observed in the experimental analysis, SMA helical springs are subjected to large displacements. The W-Spring has initial length of approximately 6 mm and hence, the maximum value of prescribed displacement of 40mm represents 8 times the original length. On the other hand, the S-Spring has initial length of approximately 10 mm and therefore the spring is subjected to a 12 times increase of its initial length.

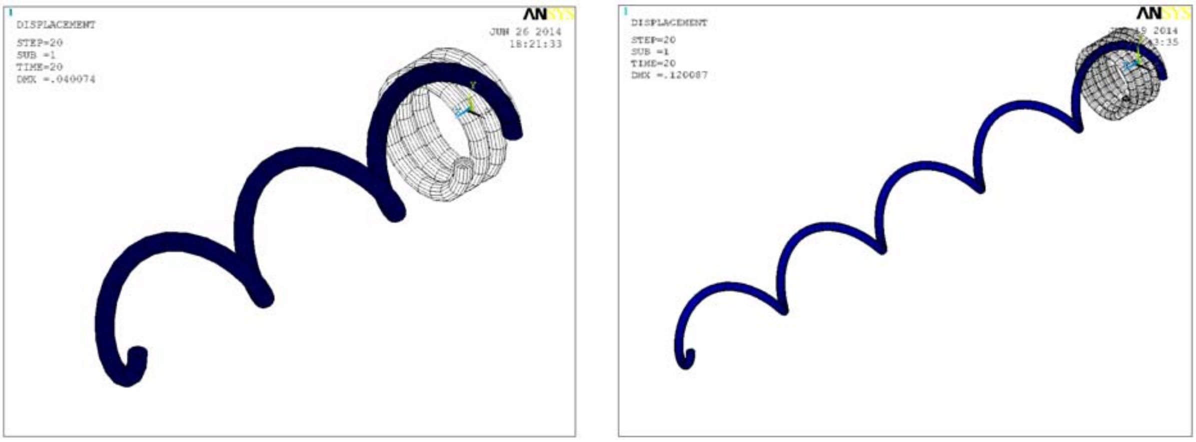

(a) (b)

Figure 5. SMA helical spring initial and deformed configurations: (a) W-Spring (40 mm maximum displacement) and (b) S-Spring (120 mm maximum displacement).

Figure 6 shows the *von Mises* equivalent stress distribution and the martensitic volume fraction for the W-Spring. Similar distributions are observed for the S-Spring. Results show just the central coils, avoiding boundary effects by removing the two end coils. Stress field presents a typical distribution of helical springs, being associated with a combination of torsion and shear internal loads acting in the cross section. Since a torque in cylindrical bodies promotes a shear stress distribution with zero values at the center with a maximum value at the surface, values of either *von Mises* equivalent stress or martensitic volume fraction are maximum at the cylinder surface. Nevertheless, it is important to note that equivalent stresses and martensitic volume fraction distribution along the wire diameter do not present a symmetrical distribution. This is a consequence of curvature effect and higher values of stresses and martensitic volume fraction are observed near to spring longitudinal axis (Mirzaeifar *et al.*, 2011).

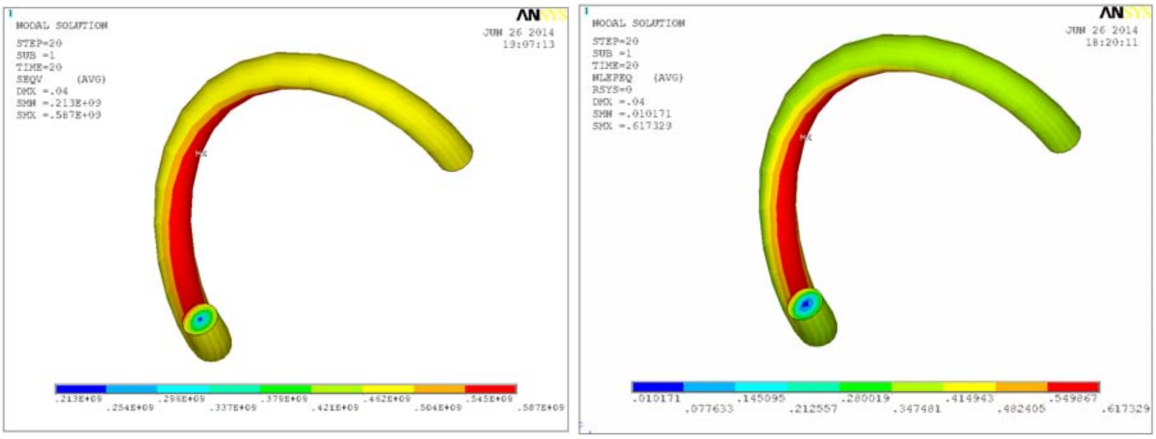

(a) (b)

Figure 6. (a) *von Mises* equivalent stress distribution and (b) martensitic volume fraction distribution for W-Spring (40 mm maximum displacement).

The effect of geometric nonlinearity is now of concern. A comparison between numerical results considering two distinct models is performed: GL - geometric linear model, neglecting nonlinear geometrical effects; and GNL - geometrical nonlinear model. This can be achieved through the command NLGEOM in the ANSYS computational package. Once again, it is important to point out that the SMA constitutive model does not consider different elastic moduli for austenite and martensite. Therefore, the model does not capture the stiffness change observed in experimental tests. Nevertheless, the model has a good agreement with the experimental data being an appropriate tool to evaluate the effect of geometric nonlinearities in the spring stiffness. Figure 7a shows results for both springs considering both models for each spring. The W-Spring analysis adopts a maximum prescribed displacement of 64 mm. On the other hand, the S-Spring analysis adopts a value of 175 mm value. Under these assumptions, for the GNL model, both springs present maximum values of von Mises equivalent stress and martensitic volume fraction of 1280 MPa and 100%, respectively. It is clear that geometric nonlinearities induce changes in the martensitic phase, reaching situations observed in experimental tests. This is evident observing that S-Spring has more pronounced changes in the spring stiffness when compared with W-Spring, exactly as pointed during experimental tests.

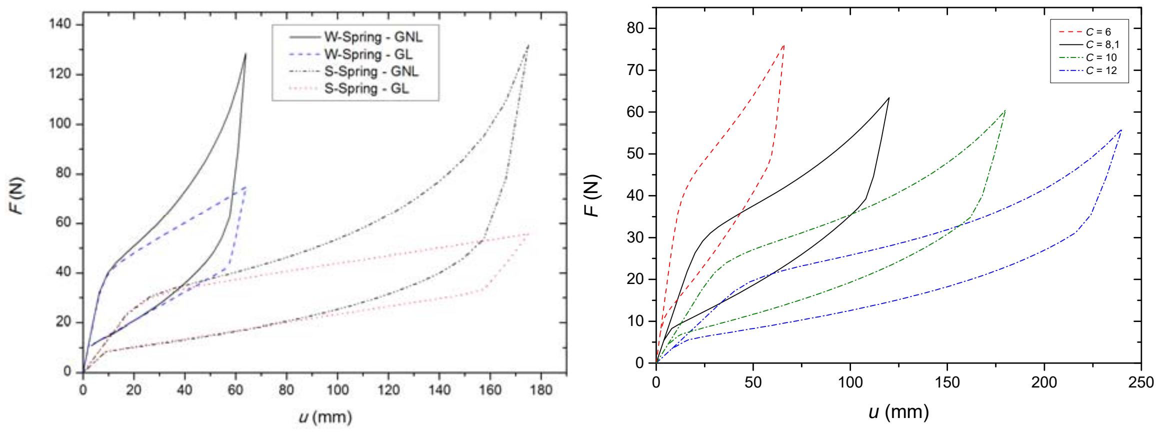

(a) (b)

Figure 7. (a) Effect of the geometric nonlinearities for W-Spring and S-Spring considering two distinct models: geometric linear (GL) and geometric nonlinear (GNL). (b) Effect of the spring index on the geometric nonlinearities: force-displacement curves

Since the spring index (C) is usually employed to quantify the effect of the geometric nonlinearity, numerical simulations considering different indexes are now in focus. The idea is to define the S-Spring as a reference situation (d = 1.7mm; D = 13.8mm; N = 5), with a spring index C = 8.1. Three other springs with different spring indexes are treated considering the variation of external diameter. Therefore, four spring indexes are investigated: 6; 8.1 (S-Spring); 10; 12. Figure 7b presents results related to these four situations with similar loading levels (maximum values for *von Mises* equivalent stress and martensitic volume fraction of approximately 600 MPa and 62%, respectively). Figure 8 shows that the increase of the spring index C tends to increase the stiffness variation, represented by the ratio K_M/K_A. Larger index values are associated with stronger geometric nonlinearity effects. Therefore, the larger geometric nonlinearity effects are present in the spring with the larger C value (12).

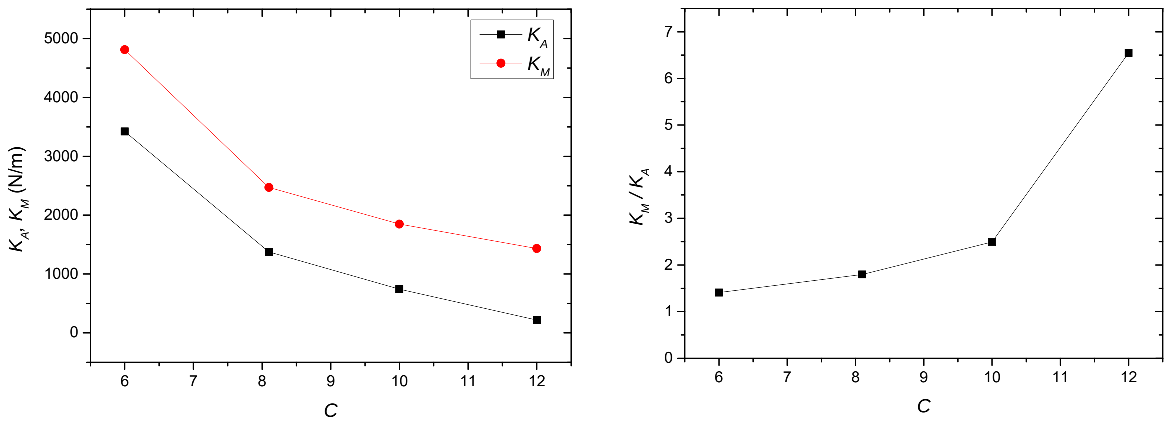

Figure 8. Effect of the spring index on the geometric nonlinearities: stiffness changes.

4. CONCLUSIONS

This paper deals with an investigation of nonlinear geometric effect on the mechanical behavior of SMA helical springs. Initially, SMA wires characterization is presented. Afterward, a discussion of design and manufacturing of SMA springs are performed. Experimental tensile tests are then carried out showing the nonlinear geometric influence. Results show the change of austenitic and martensitic stiffness due to geometric influence. Two different springs are built from SMA wires, defining a spring with weak nonlinear geometric influence, named W-Spring, and another one with strong nonlinear geometric influence, S-Spring. Tensile tests show that W-Spring has $K_A > K_M$, while S-Spring presents $K_A < K_M$. Since shear modulus is $G_A > G_M$ for both cases, this stiffness difference is due to geometrical nonlinearities. Finite element analysis is performed in order to confirm this general conclusion. Two different models are employed for this analysis: geometric linear and geometric nonlinear. Results confirm conclusions obtained from experimental data. In addition, an analysis related to spring index shows how the geometric nonlinearity can be quantified. On this basis, results show that it is important to contemplate the coupling between constitutive and geometric nonlinearities in the design of SMA helical springs.

5. ACKNOWLEDGEMENTS

The authors would like to acknowledge the support of the Brazilian Research Agencies CNPq, CAPES and FAPERJ and through the INCT-EIE (National Institute of Science and Technology - Smart Structures in Engineering) the CNPq and FAPEMIG. The Air Force Office of Scientific Research (AFOSR) is also acknowledged.

6. REFERENCES

Aguiar, R. A. A., Savi, M. A. and Pacheco, P. M. C. L., 2010. "Experimental and numerical investigations of shape memory alloy helical springs". *Smart Materials and Structures*, Vol. 19, pp.025008

Attanasi, G., Auricchio, F. and Urbano, M., 2010. "Theoretical and experimental investigation on SMA superelastic sprigs". *Journal of materials Engineering and Performance*, Vol.20, pp. 706-711.

Auricchio, F., Taylor, R.L. and Lubliner, J., 1997. "Shape-Memory Alloys: Macromodeling and Numerical Simulations of the Superelastic Behavior". *Computational Methods in Applied Mechanical Engineering*, Vol.146 , pp.281-312.

Bundhoo, V. Haslam, E., Birch, B. and Park, E. J., 2009. "A Shape Memory Alloy-Based Tendon-Driven Actuation System for Biomimetic Artificial Fingers, Part I: Design and Evaluation". *Robotica*, Vol. 27, pp. 131-146.

Case, L., Kreiner, Z., Redmond, J. and Trease, B., 2004. "Shape memory alloy shape training tutorial". *Smart Materials and Structures*, ME559.

Hartl, D. J., Lagoudas, D. C., Calkins, F. T. and Mabe, J. H., 2010. "Use of a Ni60Ti Shape Memory Alloy for Active Jet Engine Chevron Application: I. Thermomechanical Characterization". *Smart Materials and Structures*, Vol. 19, n. 20, pp. 1-14.

Lagoudas, D.C., 2008. *Shape Memory Alloys - Modeling and Engineering Applications*. Springer.

Liang, C., Rogers, C.A., 1997. "Design of shape memory alloy springs with applications in vibration control". *Journal of Intelligent Material Systems and Structures*, Vol. 8, pp.314-322.

Machado, L.G. and Savi, M.A., 2003. "Medical applications of shape memory alloys. *Brazilian Journal of Medical and Biological Research*, Vol. 36, pp. 683-691.

Min An, S., Ryu, J., Cho, M. and Cho, K.J., 2012. "Engineering design framework for a shape memory alloy coil spring actuator using a static two-state model". *Smart Materials and Structures*, Vol. 21, pp.1-16.

Mirzaeifar, R., DesRoches, R. and Yavari, A., 2011. "A combined analytical, numerical, and experimental study of shape-memory-alloy helical springs". *International Journal of Solids and Structures*, Vol. 48, p.611–624.

Paiva, A. and Savi, M.A., 2006. "An Overview of Constitutive Models for Shape Memory Alloys". *Mathematical Problems in Engineering*, Vol. 2006, Article ID56876, pp.1-30, 2006.

Paiva, A., Savi, M.A., Braga, A.M.B. and Pacheco, P.M.C.L., 2005. "A Constitutive Model for Shape Memory Alloys Considering Tensile-Compressive Asymmetry and Plasticity". *International Journal of Solids and Structures*, Vol. 42, n.11-12, pp.3439-3457.

Savi, M.A., Pacheco, P.M.C.L., Garcia, M.S., Aguiar, R.A.A., Souza, L.F.G. and da Hora, R.B., 2015. "Nonlinear geometric influence on the mechanical behavior of shape memory alloy helical springs". *Smart Materials and Structures*, Vol. 24, p. 035012.

Spinella, I. and Dragoni, E., 2010. "Analysis and Design of Hollow Helical Springs for Shape Memory Actuators". *Journal of Intelligent Material Systems and Structures*, Vol. 21, pp.185-199.

Shigley, J.E., 1986. *Mechanical Engineering Design*, McGraw Hill.

Sung-Min, A., Junghyun, R., Maenghyo, C. and Kyu-Jin, C., 2012. "Engineering design framework for a shape memory alloy coil spring actuator using a static two-state model". *Smart Materials and Structures*, Vol. 21, 055009 (16 pp).

Tobushi, H. and Tanaka, K., 1991. "Deformation of a shape memory alloy helical spring". *JSME International Journal*, Series I, Vol. 34, pp. 83–89.

Toi, Y., Lee, J.B. and Taya, M., 2004. "Finite element analysis of superelastic, large deformation behavior of shape memory alloy helical spring". *Computer and Structures*, Vol. 82, pp.1685-1693.

7. RESPONSIBILITY NOTICE

The authors are the only responsible for the printed material included in this paper.